Direct Molecular Imaging of NO Monomers and Dimers and a Surface Reaction on Ag{111}†

C. I. Carlisle and D. A. King*

Department of Chemistry, University of Cambridge, Lensfield Road, Cambridge CB2 1EW, UK

Received: September 19, 2000; In Final Form: January 14, 2001

Molecular and atomic resolution STM images are presented of NO monomers and dimers and the reaction products of the dimer thermal decomposition, N_2O and O, on a Ag{111} surface. The weakly chemisorbed NO monomer is formed at low coverages and temperatures between 4 and 65 K and is imaged as a 0.25 Å deep depression. Continued adsorption leads to multilayer dimer cluster formation at 4 K and smoother multilayer dimer packing at 65 K, with imaging of each component of some of the dimers in the top layer. Removal of the multilayer by evacuation or heating leaves the dimer chemisorbed layer, where each dimer is imaged as a protrusion. Large domains of four different ordered phases are present, which we designate as α, β, χ, and δ. This layer is quite stable at 65 K. Images including clean patches of Ag{111} showing atomic resolution of the top Ag layer enable us to present structures for each of the dimer phases, with full site assignments. The dimers are adsorbed across bridge sites at low coverage and across bridge and an atop to 3-fold site at the highest coverage, 0.25 ML. On heating to 105 K, the dimer phases are largely converted to two new ordered phases, each of which is a mixed N_2O + O phase. Some residue of the $\beta(NO)_2$ phase remains, however, indicating that it is the least reactive phase. A mechanism for the dissociation involving thermal excitation of the hindered NO rotation about the N−N axis is consistent with the reactant-to-product image sequences. Further heating to 125 K invokes N_2O desorption, leaving a residual silver oxide ring structure, which is a precursor to the stable Ag{111}-$p(4\times4)$-oxide structure.

1. Introduction

Interest in the adsorption of NO on Ag{111} stems both from the important implications in heterogeneous catalysis and the unusual surface chemistry displayed. Numerous studies have been undertaken in an attempt to elucidate the observation that no reaction takes place on the surface at room temperature, but there is a facile low-temperature reaction in which $N_2O_{(a)}$ is produced at ∼80 K.[1−10] This low-temperature reaction contradicts the notion that Ag is a relatively unreactive substrate with weak substrate−adsorbate interactions. Two different mechanisms have been put forward in order to explain the observations. The first simply involves the partial dissociative adsorption of NO below ∼80 K,[3] followed by reaction between NO and N to produce N_2O. This provides no explanation for the absence of reactivity at room temperature. An alternative mechanism has more recently been presented involving the formation of $(NO)_2$ dimers at low temperatures.[4−7] Dimer formation was experimentally observed and characterized at temperatures below 60 K by Brown et al.[6] using near-edge X-ray adsorption fine structure (NEXAFS) and reflection absorption infrared spectroscopy (RAIRS). On heating to higher temperatures the transformation to adsorbed N_2O and O adatoms was also characterized by RAIRS. Accurate density functional theory (DFT) slab calculations confirm the formation of the dimer on Ag{111}[7,10] and show that substrate mediation strengthens the N−N bond in the dimer and weakens the N−O bond, thus leading to the dissociation products $N_2O_{(a)}$ and $O_{(a)}$.[11]

Studies have also indicated the presence, at low temperatures, of NO dimers on Cu{110}[12] and Cu{111}[13] and N_2O formation. For Cu{111}, monomers form at low to medium coverages and $(NO)_2$ forms at higher coverages. Brown and King have recently reviewed the chemisorption of NO on metal single-crystal surfaces.[14]

The first observation of $(NO)_2$ dimer formation on Ag{111} was within physisorbed multilayers formed at low temperatures, by Behm and Brundle.[1] The experiments were carried out at 25 K using X-ray photoelectron spectroscopy (XPS) and TPD with further support from a theoretical study of their XPS data. Brown et al. then went on to demonstrate $(NO)_2$ dimer formation in the submonolayer regime using RAIRS.[5] A characteristic IR absorption band at 1860 cm^{-1} is attributed to the dimer. On increasing the temperature, it attenuates in favor of two peaks at 1260 and 2229 cm^{-1}, attributed to the formation of N_2O. The completion of the $(NO)_2$ to N_2O reaction was found to occur between 87 and 92 K, while N_2O desorption was observed at 117 K. Additional adsorption of NO at 90 K onto a substrate occupied by N_2O provided evidence for a stabilization of the $(NO)_2$ dimer by N_2O at this elevated temperature, since no attenuation in the peak at 1860 cm^{-1} was observed with time.

A detailed study of this system was made by Ludviksson et al. using $^{14}N^{16}O$ and $^{15}N^{18}O$ isotopes in a set of thermal desorption experiments on Ag{111} deposited on Ru{001}.[4] Adsorption of NO between 75 and 100 K produced $N_2O_{(a)}$ and $O_{(a)}$. The N_2O produced in this manner desorbed at 125 K. However, N_2O adsorbed on to clean Ag{111} at 70 K desorbed at 85 K, while on O-precovered Ag{111}, the onset of desorption was seen to occur at slightly higher temperature of 95 K. From the latter result, the presence of O is clearly a contributing factor to the stabilization of N_2O but does not account fully for the increase to 125 K, and therefore, stabiliza-

† Part of the special issue "John T. Yates, Jr. Festschrift".

10.1021/jp0033871 CCC: $20.00
Published on Web 03/14/2001

tion was attributed to a further surface species, such as NO_2 and other possible byproducts of the reaction. No clear account of the coverage of O and its adsorption state was given for the precovered Ag{111} substrate.

Here we present the first direct molecular resolution images of the adsorbate structures formed with NO adsorption on Ag{111} at 4−130 K. The NO monomer at 4 K; the $(NO)_2$ dimer; and the products of its surface decomposition, N_2O and O, have been imaged, a range of ordered structures has been directly characterized in real space, and the adsorption sites have been assigned.

2. Experimental Section

Experiments were carried out in an ultrahigh vacuum system housing a low-temperature STM (Omicron) described in detail elsewhere.[15] The STM is designed to operate at 4 K, 77 K, and room temperature. Sample heating from 4 K is achieved using a resistive heater at the STM head with subsequent surface quenching and imaging at 4 K. Heating from 77 K requires the removal of the liquid nitrogen cryogen followed by dry nitrogen gas flow through the cryostat until the desired temperature is observed at the sample. Subsequent quenching to 77 K for imaging is achieved by refilling with liquid nitrogen.

A Ag{111} crystal, cut to within 0.5° of the {111} plane, was prepared by repeated cycles of ion sputtering and annealing. Argon was used at a background pressure of 5×10^{-5} mbar for sputtering at a sample temperature of 600 K, followed by sample annealing at 780 K. Prior to dosing, the LEED pattern showed a clean, sharp (1×1) structure; no significant impurities were seen with Auger analysis, and the STM showed large, clean, and relatively defect-free terraces.

NO was dosed using a simple molecular beam doser with the crystal at the base temperature of 4 K.[15] For experiments conducted at 77 K and above, NO was background-dosed through a doorway in the heat shield cups surrounding the STM head. Both the STM and preparation chamber were maintained at a base pressure of 1×10^{-10} mbar, and an etched W tip was used for imaging.

3. Results and Discussion

3.1. Temperature Correlation with the Work of Brown et al.[5,6].

In the following, significant changes in the appearance of the STM images are associated with specific temperature ranges. Although these ranges are similar to those recorded by Brown et al.,[5,6] they are not identical, and errors must be associated with the temperature measurements. To provide a correlation between these two sets of results, an initial overall comparison is made here between the two data sets.

(i) On heating between 65 and 77 K, three-dimensional clusters associated with a multilayer produced by the adsorption of NO at 4 K give way to ordered saturated overlayers. These structures appear to be composed of just one type of adsorbate and remain stable for long periods of time at 77 K. Brown et al.[5] reported multilayer $(NO)_2$ desorption yielding a monolayer of $(NO)_2$ on heating to 63 K, identified by the growth of the 1860 cm^{-1} infrared adsorption peak.

(ii) On heating to between 77 and 105 K we find new ordered overlayers, composed of two contrasting adsorbates in a 1:1 ratio. Brown et al. observed an attenuation of the 1860 cm^{-1} dimer band and simultaneous growth of the two N_2O bands at 1260 and 2229 cm^{-1}, at temperatures greater than 70 K. The production of N_2O and O was found to be complete at 90 K.

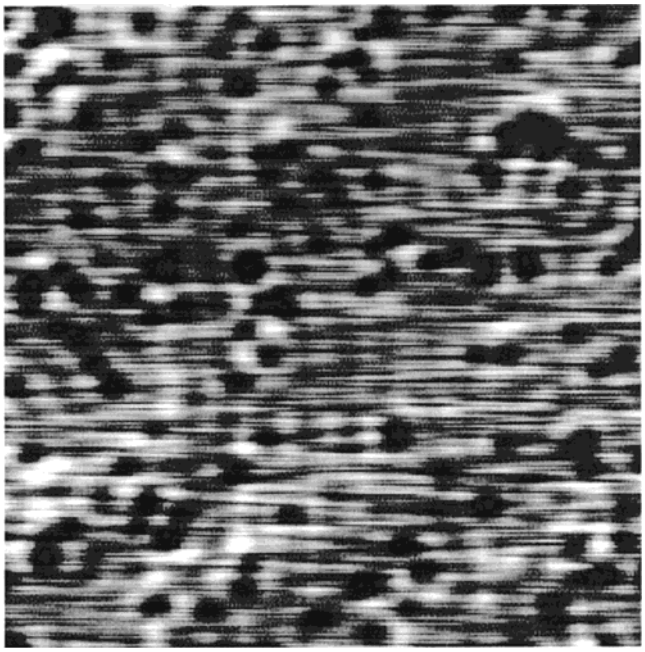

Figure 1. A 500 Å × 500 Å low coverage (0.01 ML) image of NO monomers at 4 K. NO appearance is a circular depression in the STM image, 13 ±3 Å in diameter and 0.2 ±0.05 Å in depth. The image was recorded with a bias of 28 mV and a 0.67 nA tunneling current.

(iii) The ordered overlayers associated with N_2O and O at 105 K disappear on heating between 110 and 130 K, in line with the measurements of Brown et al. for which the onset of N_2O desorption was observed at 117 K.

Clearly there is a correlation between these three sets of results, despite some discrepancy between the recorded temperatures. The main discrepancy lies in our observation of the $(NO)_2$ monolayer at 77 K. At this temperature the overlayer structures, observed by STM, remain stable over a 24-h period, unlike the RAIRS data, which predicts a relatively fast conversion to N_2O and O above 70 K. At 77 K, thermal equilibrium in the liquid-nitrogen-shrouded STM of the present instrument is readily achieved, and the temperature has been accurately calibrated. Likewise, a highly stable 4 K temperature recording is obtained with liquid helium in the cryostat. The apparatus only allows for slow heating, as opposed to relatively fast heating rates in the RAIRS experiments,[5,6] where the thermocouple was not in direct contact with the crystal but insulated from it. In conclusion, agreement between the two data sets is achieved by deducting 7−10 K from the temperatures reported by Brown et al.[5,6] This permits the interpretation of our STM data in terms of the previously published RAIRS data.

3.2. The Adsorbed NO Monomer.

At very low coverages individual NO monomers have been resolved at 4 K on Ag{111}. Figure 1 illustrates their appearance for a coverage of just 0.02 monolayers, in which each adsorbate is identified as a 0.25 ±0.05 Å deep depression with an apparent diameter of 13 ±3 Å. Wavelike patterns beyond each adsorbate image arise from Friedel oscillations in surface states close to the Fermi level. Very low coverages of NO dosed at 65 K, with subsequent cooling to 4 K for imaging, resulted in the adsorption of NO monomers identical in appearance to those dosed at 4 K.

Despite a surface and tip temperature of just 4 K, the interaction between NO and Ag{111} is weak, such that tip-induced motion of the adsorbate is almost impossible to prevent. To obtain images of stationary NO adsorbates, both large tip/sample separations and low tip biases (<0.1 V) are required.

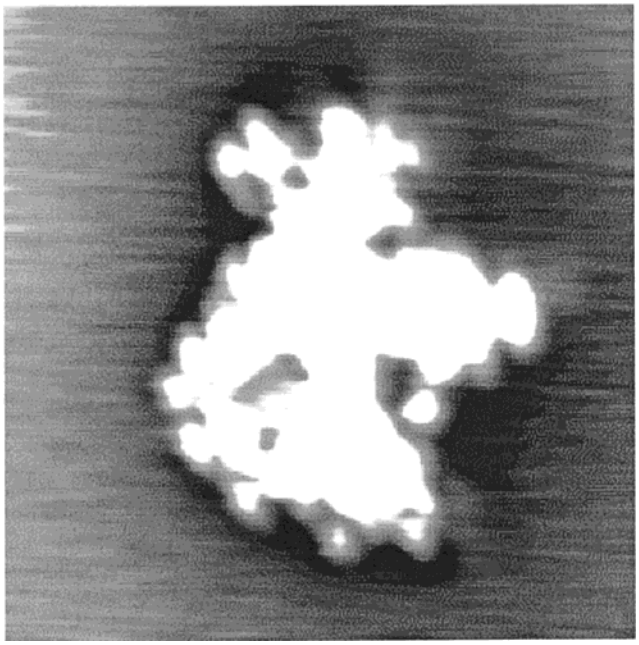

Figure 2. A 40 Å × 40 Å image of a cluster of NO at 4 K. Clusters typically appear ~0.8 Å in height. Recorded with a bias of 29 mV and a 0.1 nA tunneling current.

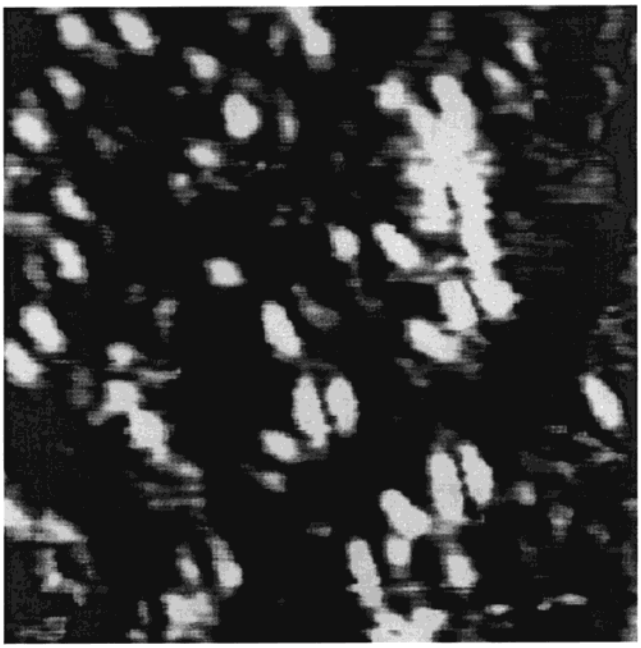

Figure 3. A 40 Å × 40 Å image of multilayer adsorption of NO at 65 K and recorded at 4 K. Clusters typically appear ~0.8 Å in height. Recorded in constant height mode, with a bias of 29 mV and a 0.1 nA tunneling current.

Even at the limit of our STM's capability, tip-induced motion of a fraction of the adsorbates in any scan area is usually observed.

The very weak interaction of the monomer with the substrate, allowing tip-induced motion at just 4 K, may be indicative of a physisorbed state. However, based on the theoretical approach of Sautet,[16] we would predict that NO adsorbed into a physisorbed state would image as a bump, and not a depression as observed. The adsorbate affects the tunneling current in two ways.[16] The first involves a reduction of the tunneling current in the close vicinity of the adsorbate, a consequence of the depletion the density of states at the Fermi level by the localized adsorbate bonding. This effect increases with an increase in the bonding interaction between adsorbate and substrate and produces a depression in the image centered on the adsorbate. The second contribution arises from polarization of the adsorbate and has a positive effect on the tunneling current as a result of tunneling directly through the adsorbate. The magnitude of this effect is determined by the degree of tip and adsorbate orbital overlap and is therefore related to the polarizability of the adsorbate. In the case of a weakly bound polarizable molecule, this contribution dominates the tunneling current, producing a protrusion at the adsorbate position in the STM image. We, however, observe the converse and conclude that the monomeric species is chemisorbed.

On the basis of a DFT slab calculation Pérez-Jigato and King[11] show that the monomeric species is a weakly bound chemisorbed state, bonding to the Ag{111} substrate through the N atom. A net charge transferral from the substrate to the adsorbate results in a negatively charged $NO^{\delta-}$ species with a low heat of adsorption of 0.5 ± 0.1 eV. We note that chemisorbed monomers have been observed on Cu{110}[12] and Cu{111}[13] at low coverages.

3.3. NO Clusters and Multilayer Dimers at Low Temperature.

With increasing NO coverage at 4 K, clustering is observed, an example of which is shown in Figure 2. Clusters appear to be three-dimensional with heights measuring 0.8 ±0.05 Å and surrounded by a dark halo, ~0.2 Å in depth. Contrast reversal results in a bright appearance in the STM image, in contrast to the depressions produced by the monomer. This can be attributed to both a change of the physisorbed state (in the multilayer) and an increase in the cluster height, dominating over the effect of NO on the local density of states.

During adsorption at 65 K, followed by quenching to 4 K to image the surface, the formation of NO monomers at low coverage is followed by multilayer formation, which often images as pairs of elongated bright features (Figure 3). These features are separated by ~2.3 Å, which is very close to the N−N bond length of the dimer in the condensed phase, which is 2.18 Å.[17] These images might correspond to the dimers characterized in the multilayer.[1,6]

Heating the system to 65 K for 30 min results in a loss of the three-dimensional character of the clusters. As shown in Figure 4, the image is dominated by bright features with a nearest-neighbor spacing of ~3 Å. The loss of the multilayer correlates well with the data of Behm and Brundle[1] and Brown et al.,[5] who observed multilayer desorption at 60−63 K. The features in Figure 4 are therefore attributable to a monolayer species. There is a strong correlation with the images of the chemisorbed NO monomer (Figure 1), and in keeping with Brown et al.,[5] we attribute these bright features to the chemisorbed dimer. RAIRS data show that $(NO)_2$ in the multilayer is randomly packed with respect to the N−N bond. The STM images of clusters, shown in Figure 3, complement the RAIRS data, with the observation of random orientations. Some dimers at the multilayer surface with N−N bonds parallel to the Ag surface are to be expected, which is in line with the observations made in Figure 3, where the dimers appear to be resolved into two components.

We have noted in section 3.2 above that whereas dimers are formed in the first layer after pumping away a multilayer at 65 K, NO *monomers* are observed after adsorption of NO at 65 K. We therefore conclude that the transition from the monomer to the dimer state is facilitated by removing a multilayer; it is not solely dependent on temperature. As described in the next

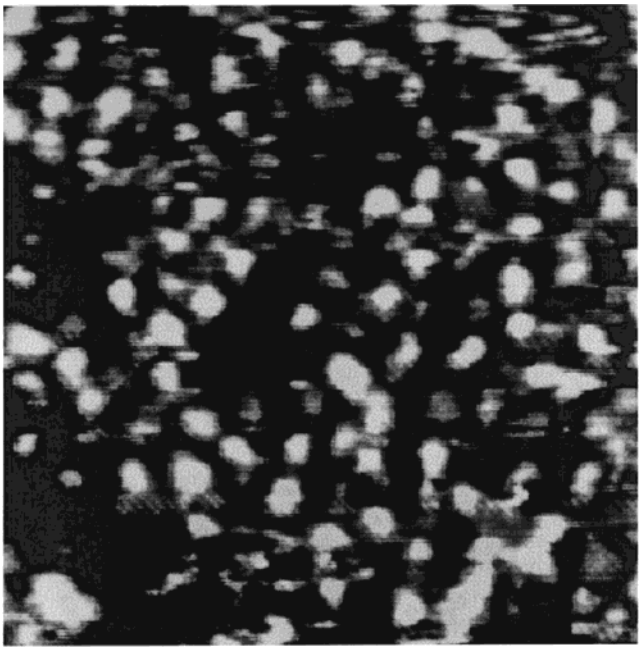

Figure 4. A 40 Å × 40 Å image of NO at 4 K following a 30 min anneal to 65 K. Recorded in constant height mode, with a bias of 140 mV and a 0.14 nA tunneling current.

section, ordered structures can also be formed by the chemisorbed dimer.

3.4. Ordered Dimer Structures.

Background dosing with ~10 langmuirs of NO at 77 K produces images showing large areas of well-ordered chemisorbed structures. Four different very well ordered overlayer structures are observed within large structural domains, with adsorbates imaging as ~0.8 Å high protrusions, in contrast to the depressions characteristic of the monomer. Examples of each of the structure types or phases observed are shown in Figure 5, which we designate as α, β, χ, and δ phases. Corresponding models are shown in Figure 6 and are explained below. Structure α is the least prevalent, while structure δ is dominant, covering roughly half the surface.

Neighboring domains, ~100 Å in diameter, tend to share the same structure; an example of an antiphase domain boundary for the β phase is shown in Figure 7. This figure provides an important new piece of structural information. The β structures on either side of the domain boundary are at 30° to each other. On this basis we can rule out exclusive occupation of high-symmetry dimer sites, such as the atop-to-atop bridge site, since the square array β structure would then only form antiphase domain boundaries with a 60° rotation between phases. Ordering is good, though not perfect, and image appearance is dependent upon tip structure. Although tip changes occur, the regularity of the unit cell is conserved, allowing a confident structure analysis. No two different phases have ever been observed within the same image. While domain boundaries have been imaged, we have not been able to image boundaries between two differing phases; it appears that one domain type dominates large areas relative to our typical scan areas of between 10 and 1000 Å.

All images of the dimers shown in Figure 5 consist of similar elliptical protrusions, approximately 5 Å in length. Each is readily attributed to just one type of adsorbate, the dimer. These bright features are sometimes resolved as two neighboring peaks separated by a distance close to the Ag−Ag bond length of 2.89 Å (see structure χ in Figure 5), reflecting the symmetry of the underlying Ag{111} lattice. No changes have been observed

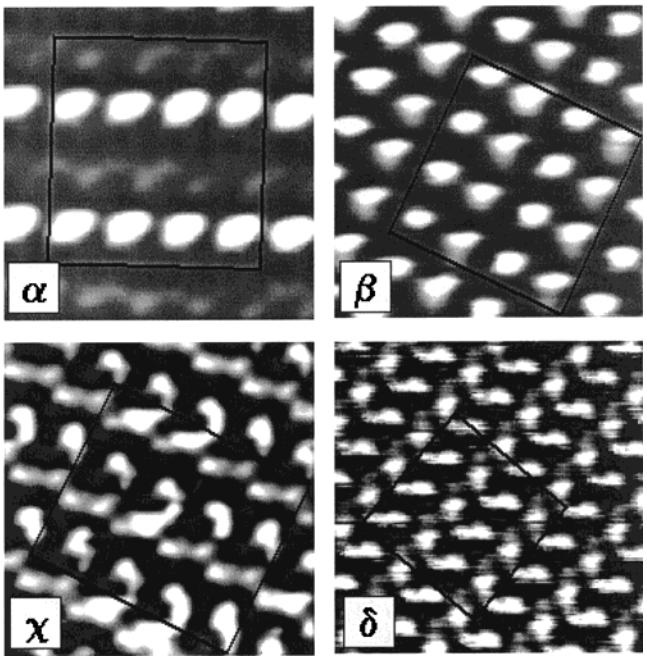

Figure 5. STM images of the four phase structures of $(NO)_2$ dimers on Ag{111} at 77 K. Each dimer appears as an elongated bright feature. Each image has had the minimum amount of correction and therefore a small amount of distortion remains evident from image to image. All were recorded with a 1 V bias and a 1 nA tunneling current. (a) A 30 Å × 30 Å area with a local coverage of 0.125 ML of $(NO)_2$. (b) A 33 Å × 33 Å area with a local coverage of 0.25 ML of $(NO)_2$. (c) A 30 Å × 30 Å area with a local coverage of 0.25 ML of $(NO)_2$. (d) A 44 Å × 44 Å area with a local coverage of 0.25 ML of $(NO)_2$.

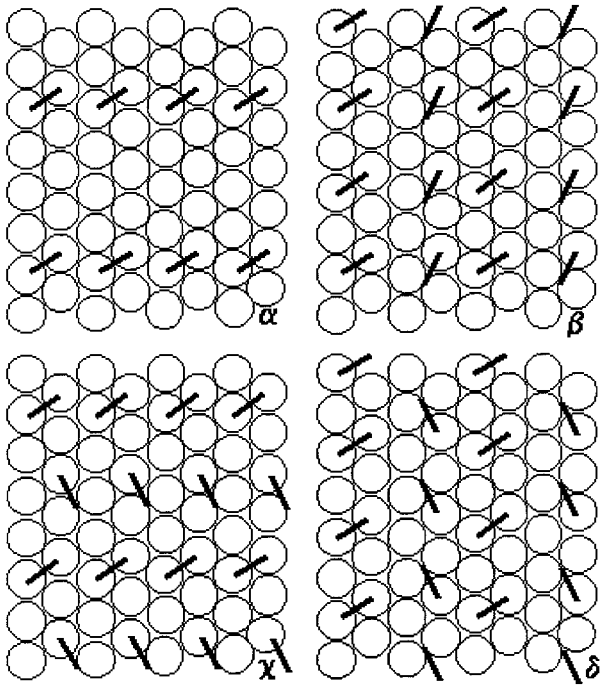

Figure 6. Models α, β, χ, and δ represent structures for the corresponding phases in the areas marked by squares in Figure 5. Open circles represent atomic positions of the underlying Ag{111} lattice, while short lines mark the direction of elongation in the dimer-induced STM features.

in these overlayers over periods of up to several hours. The dimer remains stable at 77 K.

By overlaying the Ag{111} lattice of the correct size and orientation, we were able to derive the models presented in Figure 6 for the four phases. Images of the atomically resolved

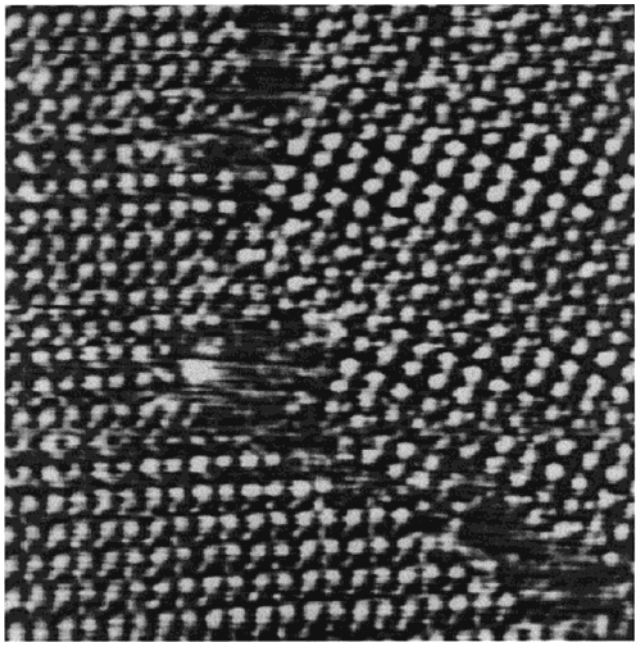

Figure 7. A 130 Å × 130 Å STM image of an antiphase domain boundary of the β phase (1 V, 1 nA), showing an angular rotation of 30° between phases across the boundary.

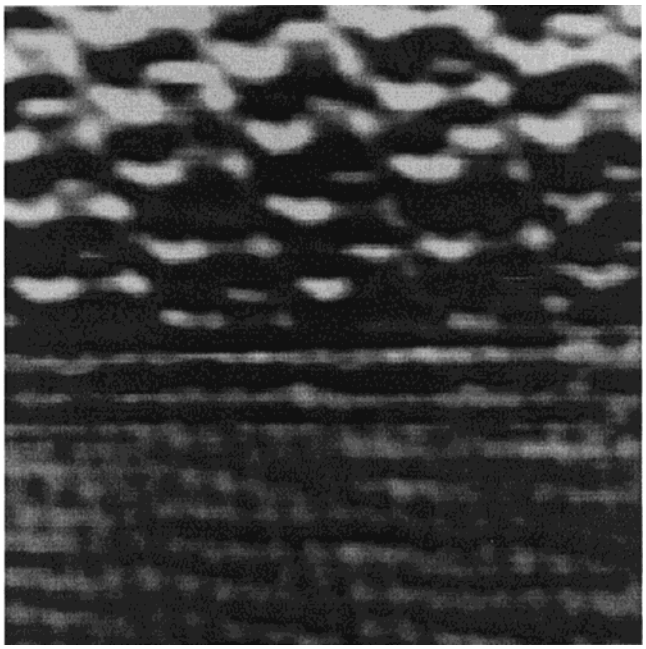

Figure 8. A 130 **Å** × 130 Å STM image of simultaneous atomic resolution of clean Ag{111} (bottom) and of the δ phase (top) within the same image (1 V, 1 nA).

Ag{111} lattice are readily obtained[18] under similar tunneling conditions. On several occasions, areas of clean Ag{111} and areas of the dimer overlayers have been resolved within the same STM image. Site symmetry can therefore be achieved by the extrapolation of the atomically resolved clean Ag{111} lattice directly onto the overlayers. An example of the simultaneous resolution of Ag{111} and the δ phase structure is shown in Figure 8. Further support for our assignments for the structures of the α and δ phases shown in Figure 9. Overlaying the models directly on to the corresponding phases highlights the coincidence between the model Ag{111} lattice with atom-sized features resolved between the dimers. We have obtained simultaneous atomic resolution of Ag atoms in the Ag{111}

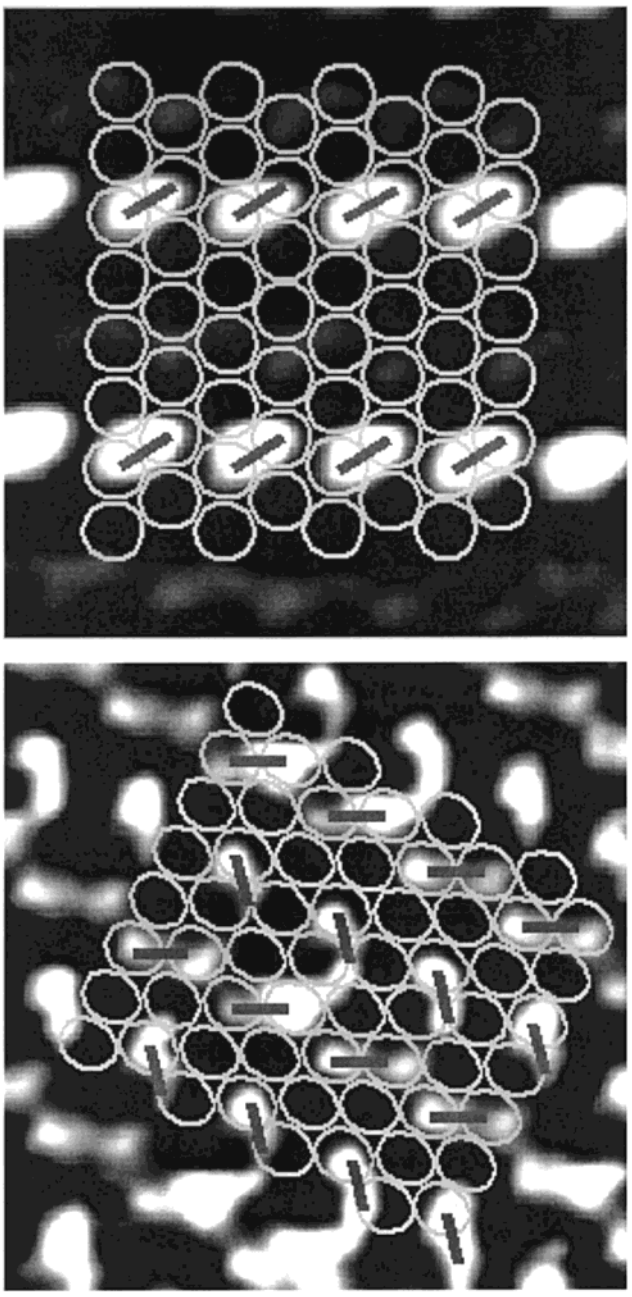

Figure 9. Models of the phase structures α and χ from Figure 6 superimposed on the corresponding STM images from Figure 5. Alignment of the Ag atoms of the models with the Ag atomic resolution apparent in these images supports the interpretations.

substrate and the dimer overlayer, confirming the site assignments for the models shown in Figure 6. In these models the black lines indicate the direction of the elongated features and are related to the dimer adsorption geometry below.

The α phase corresponds to an $(NO)_2$ coverage of 0.125 ML, and the unit cell can be described in matrix notation as Ag{111}-$\begin{pmatrix} 2 & 1 \\ 0 & 4 \end{pmatrix}$-$(NO)_2$. The other three overlayers all correspond to an $(NO)_2$ coverage of 0.25 ML, and β, χ and δ and an interconversion of these phases can be achieved by a rotation of the dimers in an ordered fashion between neighboring bridge sites. The unit cell of the χ phase is the same as the α phase, i.e., Ag{111}-$\begin{pmatrix} 2 & 1 \\ 0 & 4 \end{pmatrix}$-$(NO)_2$, while β and δ can both be described as Ag{111}-$\begin{pmatrix} 4 & 0 \\ 0 & 2 \end{pmatrix}$-$(NO)_2$.

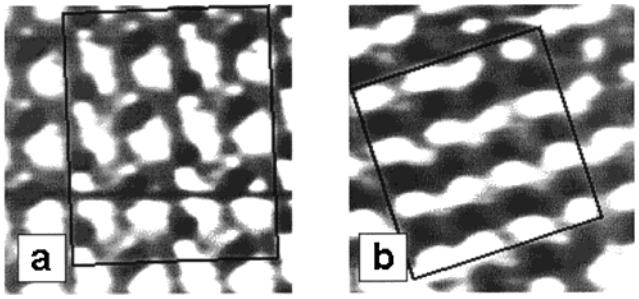

Figure 10. STM images of the two phase structures of N_2O + O adlayers on Ag{111} at 77 K. Each N_2O appears as a bright feature, while O appears as an adjacent dark feature. Each image has had the minimum amount of correction and therefore a small amount of distortion remains evident from image to image. All were recorded with a 1 V bias and a 1.8 nA tunneling current. (a) A 30 Å × 30 Å area originating from the reaction of phase δ (b) A 30 Å × 30 Å area originating from the reaction of phase β.

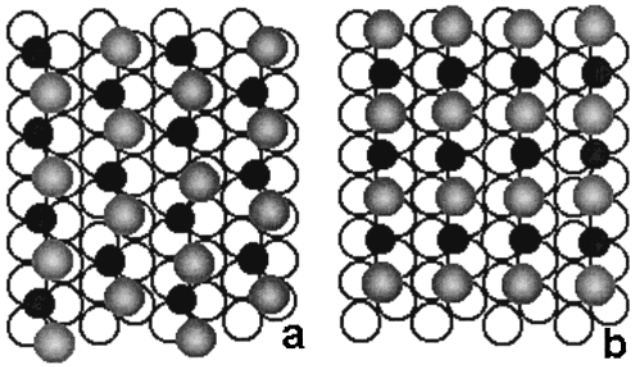

Figure 11. Models a and b represent the corresponding phases present in Figure 10 within the marked squares. Open circles correspond to the underlying Ag{111} lattice, while light circles correspond to N_2O and dark circles to O. Although O adsorption is assigned to 3-fold hollow sites, the site of N_2O is not well-defined.

There is a clear tendency for the dimers to distribute themselves such that the $(NO)_2$ coverage is maintained at 0.25 ML; only the α phase, observed infrequently, is at 0.125 ML. The images shown in Figures 5 and 6 therefore correspond to a macroscopic coverage close to 0.25 ML of $(NO)_2$. The coexistence of phases β, χ, and δ at 0.25 ML and 77 K clearly demonstrates that the structures are almost energetically degenerate; the dominance of the δ phase indicates a slight preference for this structure. The substrate needs to be carefully annealed, just below the temperature at which the reaction to N_2O and O occurs, to allow this energetically most stable phase to grow and dominate the surface structure. Within each domain the structure is coherently maintained.

In the α structure (local coverage 0.125 ML), all dimers occupy bridge sites, but for the remaining structures (local coverage 0.25 ML), bridge site occupation is accompanied by a low symmetry atop to 3-fold hollow site. This must arise from a repulsive destablization of the additional dimer adsorbate due to near-neighbor interactions. We conclude that the bridge site is favored at low coverages.

3.5. The Reaction $(NO)_2 \rightarrow N_2O_{(a)} + O_{(a)}$.

The dimer phases, formed by the adsorption of NO at 77 K, react on being heated to 105 K for ~5 min to produce $N_2O_{(a)}$ and $O_{(a)}$.[5] Imaging was carried out after quenching to a base temperature of 77 K. In addition to the persistence of the β phase after heating to 105 K, two new structures are observed. These new overlayer structures are shown in Figure 10, and each is clearly composed of two different images, one appearing as a dark depression, which we assign to the O adatoms, and the other appearing bright, assigned to N_2O. Phase structure "a" is the more abundant of the two structures, while approximately 30% of the surface is still occupied by dimers in phase β. The other $(NO)_2$ phases, α, χ, and δ, were not observed after heating, which implies that these structures are more readily converted to the N_2O + O structures.

Overlaying a Ag{111} lattice of the correct dimensions with structures in Figure 10 provides the schematic models shown in Figure 11. Since the Ag{111} lattice was not simultaneously resolved, the adsorption sites cannot be determined with certainty and these models act only as a guide. However, the chosen registry is justified below. The bright features are marked by light-filled circles and the dark features are marked by dark-filled circles.

Both of these models have a coverage of 0.25 ML for both bright and dark features, which appear in a 1:1 ratio. The two features must therefore be associated with $N_2O_{(a)}$ and $O_{(a)}$, derived from an initial $(NO)_2$ coverage of 0.25 ML. Our earlier STM observations and simulations of O on Ag{111}[15,18] confirm the assignment of the dark features to $O_{(a)}$. The expected larger polarizability of $N_2O_{(a)}$, in addition to the larger molecular size, compared to $O_{(a)}$, is consistent with N_2O appearing as a large protrusion in the STM image.

The O adatom is assigned to 3-fold coordinated sites, in line with adsorption behavior on other substrates.[19] The precise coordination geometry of N_2O cannot be assigned from these images without the use of theoretical simulations. However, a comparison of the models in Figure 5 with those in Figure 11 suggest that the N_2O + O phases "a" and "b" can be related to the δ-$(NO)_2$ phase—the most prominent—and the β phase structures, respectively. Each has the same unit cell, Ag{111}-$(^{4}0^{0}2)$, adding further support to our interpretations of the N_2O + O adlayer images.

The dominance of phase a over b can be explained in terms of the dominance of its parent dimer phase. However, the absence of further structures, related to α and χ phase structures, implies that they also react to form N_2O + O phases a and b. We have noted that the β phase persists after heating. A cooperative dimer motion to produce the reaction products N_2O + O could allow a reaction free of steric constraints for the optimal α, χ, and δ phases, whereas the β phase may be sterically constrained. A possible reaction mechanism is discussed in section 3.7 below.

3.6. Desorption of $N_2O_{(a)}$ and Formation of Silver Oxide Ring Residues.

After imaging the structure formed at 105 K, consisting of an estimated 30% dimers and 70% $N_2O_{(a)}$ + $O_{(a)}$ (Figure 10), the surface was heated to 130 K for ~5 min in order to desorb N_2O and any remaining NO. The general appearance of the surface is shown in Figure 12a. The entire surface is covered with small ringlike structures identical to those observed after the flash desorption of the $p(4\times4)$-oxygen induced reconstruction of Ag{111}.[15] These were attributed to individual ring components of the oxide structure, Ag{111}-$p(4\times4)$-O, each containing 12 silver atoms and 6 oxygen atoms, depicted in Figure 12b. The average number density of these components, expressed per surface silver atom, is found to be just ~0.02 ML, which converts into an O coverage of ~0.12 ML.

On heating the dimer adlayer, N_2O is desorbed at 125 K, which is higher than that for N_2O on clean Ag{111} (85 K) or N_2O with preadsorbed oxygen (95 K).[4] We have shown that atomic oxygen is randomly adsorbed at low coverages on Ag{111}, with a closest distance of approach of ~10 Å.[15] In

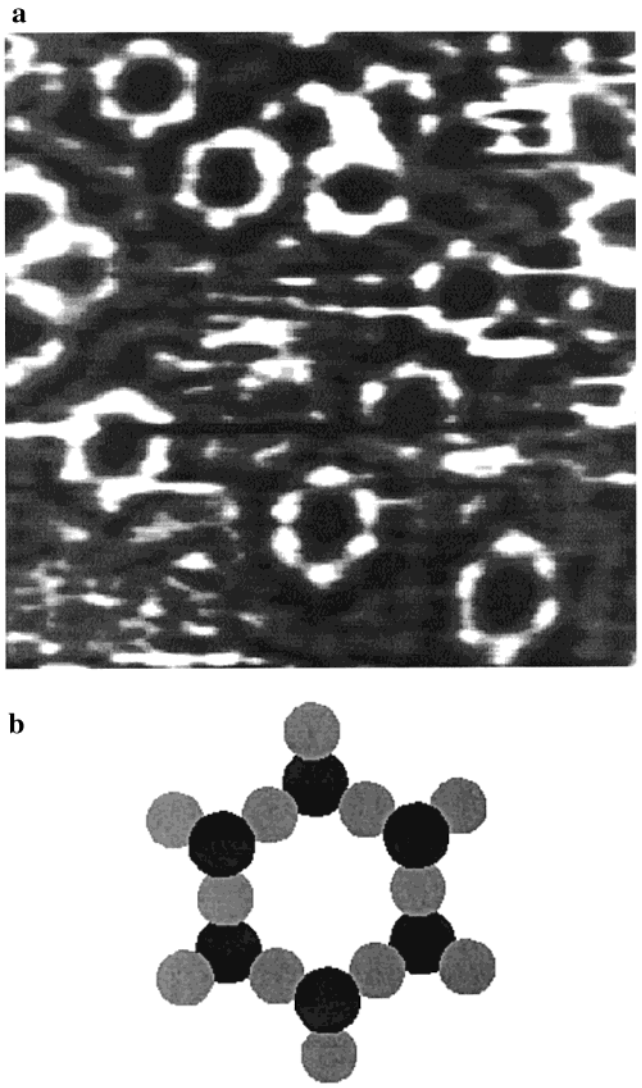

Figure 12. (a) 90 Å × 90 Å image of oxide "rings" on Ag{111} at 77 K. Their formation is a result of annealing NO on Ag{111} to 130 K. Recorded in constant height mode (1 V, 1 nA). (b) A model of an individual ring component of the $p(4\times4)$-O structure, taken from ref 15.

contrast, the present results show that $(NO)_2$ decomposition leads to a regular geometry of N_2O adsorbed molecules and O adatoms, with a coverage of 0.25 ML, which would not be mimicked by preadsorbing oxygen followed by N_2O adsorption. Attractive N_2O/O interactions are optimized in these well-ordered mixed phases, leading to the high temperature of the N_2O desorption peak at 125 K. This is further supported by the absence of any other species in the STM images, after heating to 130 K (Figure 12). Similar observations have been made by Jorgensen et al. for coadsorbed hydroxyl and oxygen on Ag{110}, for which it was found that atomic O stabilizes the hydroxyl groups via attractive lateral interactions that can extend for up to twice the lattice distance.[20]

The production of oxide rings, $Ag_{12}O_6$, was not expected given the maximum recorded temperature of only 130 K. The decomposition of a 0.25 ML $(NO)_2$ adlayer therefore provides a route to this intermediate, metastable state of O on Ag{111}, in the form of individual randomly adsorbed oxide rings. The formation is driven by the local coverage of atomic O at 0.25 ML. Above 0.05 ML, adsorbed O becomes thermodynamically unstable with respect to the $p(4\times4)$-oxide reconstruction of Ag{111}.[15] Spontaneous ring formation results from the heating of the $(NO)_2$ adlayer to 130 K, but the low temperature does not allow sufficient diffusion, for the formation of an equilibrated surface with $p(4\times4)$-O islands and atomic subsurface O_c.[15] At higher temperatures (>400 K), these rings would become unstable and break up into a two-phase system composed of islands of $p(4\times4)$-oxide and subsurface atomic O_c.

3.7. Adsorption Geometries and a Reaction Mechanism for $(NO)_2 \rightarrow N_2O + O$.

Using symmetry arguments and a detailed study of the dipole coupling observed in their RAIRS data, Brown et al. were able to determine the geometry of the $(NO)_2$ dimer.[5] In the monolayer regime the N−N bond is parallel to the surface, with DFT calculations indicating a significant through-substrate-mediated interaction which shortens this bond by 19% compared with free $(NO)_2$.[11] NEXAFS studies indicate that the N−O axis is tilted 30° with respect to the surface normal,[6,10] whereas more recent DFT calculations favor N−O bonds almost perpendicular to the substrate.[11] In particular, the calculations of Peréz-Jigato and King[11] demonstrate a strong preference for $(NO)_2$ adsorption across bridge sites, supporting the configurations shown in Figure 6. The calculated heat of adsorption is 1.34 eV per dimer, greater than that of two monomers. The increase in the N−N bonding interaction is a result of an in-phase overlap of the two neighboring π-molecular orbitals, while electron donation into the antibonding π-states results in a weakening of the N−O bond[11] and illustrates the origin behind the reaction to N_2O.

Following Brown et al,[5] low-temperature thermal excitation of the hindered N−O rotation about the N−N axis allows for one of the O atoms to contact the bare Ag surface. As bond making is initiated between Ag and O, the N−O bond further weakens to produce $N_2O_{(a)}$ and $O_{(a)}$. This model is supported by our results. Assuming that in our images the direction of elongation of the bright features is equivalent to the direction of the N−N bond, N−O rotation about this axis in the δ and β $(NO)_2$ phases allows for the deposition of O in adjacent 3-fold hollow sites, directly yielding the a and b $N_2O + O$ phases, respectively. This is demonstrated in the reactant to product models shown in Figure 13. The product models show N_2O in the geometry expected immediately after N−O bond cleavage, which is not the geometry and bonding site in the equilibrated phases (Figure 10). This process is cooperative: once the reaction of a dimer has been initiated, the product phase would grow to produce domains of the new coadsorbed structure. $(NO)_2$ overlayers that freely allow the required N−O rotation should readily react on heating, whereas those structures that hinder the motion prevent a straightforward reaction. This provides a simple reason for the lower reactivity of the β $(NO)_2$ phase.

4. Conclusions

At low coverages and with adsorption at 4−65 K, individual NO monomers are imaged at 4 K and appear as depressions in the STM image. The low barrier to diffusion, in conjunction with its appearance in the STM, leads us to conclude that the monomer is weakly chemisorbed. On increasing the coverage. 3D clusters are formed, and within this condensed phase, physisorbed $(NO)_2$ dimers exist at random orientations.

Dimers in the first layer appear as protrusions in the STM image. Four ordered chemisorbed $(NO)_2$ phases were characterized at 77 K. Three of these phases correspond to a local coverage of 0.25 ML of the dimer and one to 0.125 ML. Simultaneous imaging of clean Ag{111} areas has provided a means of making a full series of site assignments for each of these phases. Since these phases coexist and pairs of the

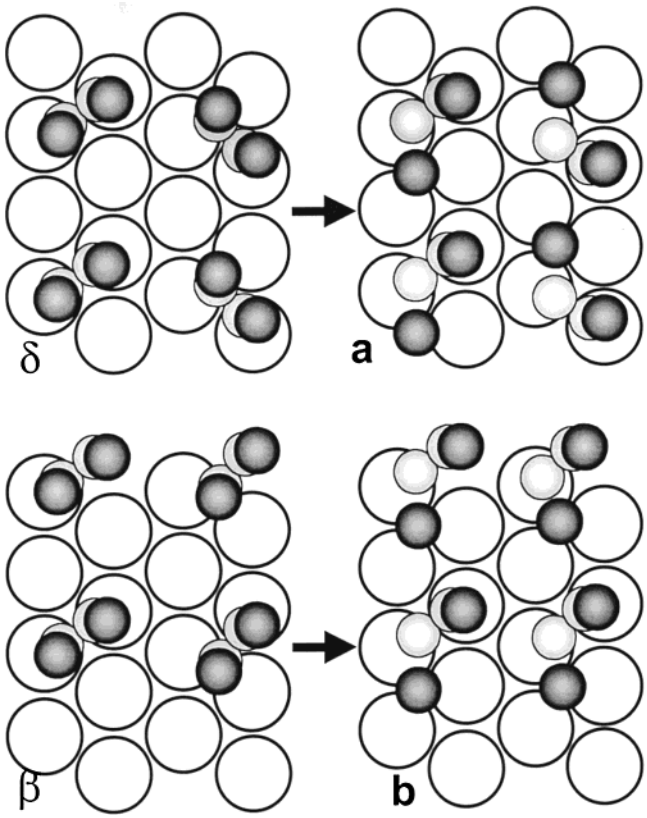

Figure 13. A schematic representing the reaction of $(NO)_2$ to N_2O + O for the δ to a phase and the β to b phase transitions, respectively. Open circles mark the underlying Ag{111} lattice, while small open circles are N and dark circles are O. The "after" diagrams show N_2O in the conformation expected on reaction and does not represent the expected geometry on imaging.

structures have the same unit cell, only a locally resolving diffraction technique would yield a full structural analysis: a standard LEED analysis would lead to ambiguities.

A reaction takes place between 77 and 105 K, in which $(NO)_2$ dimers decompose to produce $N_2O_{(a)}$ and $O_{(a)}$. These two species are readily distinguishable by STM due to opposing contrast, with $N_2O_{(a)}$ imaging bright, while $O_{(a)}$ images dark. The resultant ordered mixed overlayer structures appear to be produced by a frustrated rotation of the N−O segments of the dimer about the N−N bond, reflecting the $(NO)_2$ overlayer symmetry prior to reaction. Stabilization of N_2O on the Ag{111} substrate is a result of an attractive interaction between N_2O and $O_{(a)}$ in the well-ordered product phases formed. The intimate packing of the two species is consistent with the initial ordering of the $(NO)_2$ dimers.

On heating the product N_2O + O phases, N_2O is desorbed at 125 K, leaving a metastable ring-oxide phase. This is a new route to the formation of microscopic surface Ag_2O subunits. Condensation of these units produces the stable $p(4\times4)$-oxide phase, normally only produced at high temperatures and high O_2 pressures.

Acknowledgment. We gratefully acknowledge useful discussions with Toshiyuki Fujimoto, Matthew Webb, and Manuel Peréz-Jigato; an equipment grant from the U.K. EPSRC; and a Studentship from the EPSRC for C.I.C.

References and Notes

(1) Behm, R. J.; Brundle, C. R. *J. Vac. Sci. Technol*. **1984**, *A2*, 1040−1041.
(2) Nelin, C. J.; Bagus, P. S.; Behm, R. J.; Brundle, C. R. *Chem. Phys. Lett.* **1984**, *105*, 58−63.
(3) So, S. K.; Franchy, R.; Ho, W. *J. Chem. Phys.* **1989**, *91*, 5701−5706; **1991**, *95*, 1385−1399
(4) Ludviksson, A.; Huang, C.; Jänsch, H. J.; Martin, R. M. *Surf. Sci.* **1993**, *284*, 328−336.
(5) Brown, W. A.; Gardner, P.; King, D. A. *J. Phys. Chem.* **1995**, *99*, 7065−7074.
(6) Brown, W. A.; Gardner, P.; Pérez-Jigato, M.; King, D. A. *J. Chem. Phys.* **1995**, *102*, 7277−7280.
(7) Pérez-Jigato, M.; King, D. A.; Yoshimori, A. *Chem. Phys. Lett.* **1998**, *300*, 639−644.
(8) Jänsch, H. J.; Huang, C.; Ludviksson, A.; Rocker, G.; Redding, J. D.; Metiu, H.; Lambert, R. M. *Surf. Sci.* **1989**, *214*, 377−395.
(9) Edamoto, K.; Maehama, S.; Miyazaki, E.; Miyahara, T.; Kato H. *Surf. Sci.* **1998**, *204*, L739-L744.
(10) Pérez-Jigato, M.; Termath, V.; Gardner, P.; Handy, N. C.; King, D. A.; Rassias, S.; Surman, M. *Mol. Phys.* **1995**, *85*, 619−933.
(11) Pérez-Jigato, M.; King, D. A. Manuscript in preparation.
(12) Brown, W. A.; Sharma, R. K.; King, D. A.; Haq, S. *J. Phys. Chem.* **1996**, *100*, 12559−12568.
(13) Dumas, P.; Suhren, M.; Chabal, Y. J.; Hirschmugl, C. J.; Williams, G. P. *Surf. Sci.* **1997**, *371*, 200−212.
(14) Brown, W. A.; King, D. A. *J. Phys. Chem. B*, **2000**, *104*, 2578−2595.
(15) Carlisle, C. I.; Fujimoto, T.; Sim, W. S.; King, D. A. *Surf. Sci*. In press.
(16) Sautet, P. *Surf. Sci.* **1997**, *374*, 406−417.
(17) Lipscomb, W. N.; Wang, F. E.; May, W. R.; Lippert, E. L. *Acta Crystallogr.* **1961**, *14*, 1100−1101.
(18) Carlisle, C. I.; King, D. A.; Bocquet, M−L.; Cerdá, J.; Sautet, P. *Phys. Rev. Lett.* **2000**, *84*, 3899−3902.
(19) Starke, U.; van Hove, M. A.; Somorjai, G. A. *Prog. Surf. Sci.* **1994**, *46*, 305−319.
(20) Jorgensen, S. W.; Sault, A. G.; Madix, R. J. *Langmuir* **1985**, *1*, 526−528.
(21) Zhang, C. M.; Bartelt, M. C.; Wen, J. M.; Jenks, C. J.; Evans, J. W.; Thiel, P. A. *Surf. Sci.* **1998**, *406*, 178−193.
(22) Czanderna, A. W. *J. Phys. Chem*. **1964**, *68*, 2765−2772.